ACS NANO
Cite This: ACS Nano 2019, 13, 6992–6997
www.acsnano.org

ARTICLE

Near-Unity Light Collection Efficiency from Quantum Emitters in Boron Nitride by Coupling to Metallo-Dielectric Antennas

Xiangzhi Li, Robert A. Scully, Kamran Shayan, Yue Luo, and Stefan Strauf*

Department of Physics and Center for Quantum Science and Engineering, Stevens Institute of Technology, Hoboken, New Jersey 07030, United States

Supporting Information

ABSTRACT: The bright and stable single-photon emission under room temperature conditions from color centers in hexagonal boron nitride (hBN) is considered as one of the most promising quantum light sources for quantum cryptography as well as spin-based qubits, similar to recent advances in nitrogen-vacancy centers in diamond. To this end, integration with cavity or waveguide modes is required to enable ideally lossless transduction of quantum light states. Here, we demonstrate a scheme to embed hBN quantum emitters into on-chip arrays of metallo-dielectric antennas that provides near unity light collection efficiencies with experimental values up to 98%, *i.e.* a 7-fold enhancement compared to bare quantum emitters. Room-temperature quantum light emission in the 700 nm band is characterized with single-photon emission rates into the first lens up to 44 MHz under continuous excitation and up to 10 MHz under 80 MHz pulsed excitation (0.13 photons per trigger pulse) into a narrow output cone (±15°) that facilitates fiber butt-coupling. We furthermore provide here a direct measurement of the quantum yield under pulsed excitation with values of 6−12% for hBN nanoflakes. Our demonstrated scheme could enable low loss spin−photon interfaces on a chip.

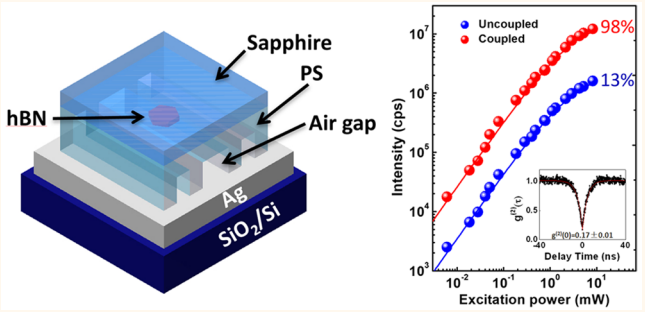

KEYWORDS: *hexagonal boron nitride, color center, metallo-dielectric antenna, single-photon source, 2D materials, quantum yield*

Recent advances in single-photon sources based on atomically thin materials are promising to enable on-chip quantum technologies.[1] Particularly, the color centers in hexagonal boron nitride (hBN) have been shown to emit single photons not only at room temperature,[2] but even under harsh environment conditions up to 800 K.[3] The color centers can be found in bulk crystals,[4,5] in monolayers grown *via* chemical vapor deposition (CVD),[2] or in solution-based nanoflakes[2,6] and need to be activated typically by thermal annealing,[2] chemical etching,[7] electron beam irritation,[8] or plasma etching.[9] The resulting wavelength distribution for the optical emission occurs over an extremely broad range spanning several hundred nm in the visible range[10] and can be partially tuned by temperature,[6] strain,[11] and the Stark-effect.[12] Significant progress has been made based on low pressure CVD growth that results in spectrally narrow wavelength distribution over only 10 nm range with a zero-phonon line (ZPL) at 580 nm.[13] Toward spatial control of hBN color center formation it was shown that substrate-induced strain can give rise to quantum emitter activation,[14] while drilling holes with a focused ion beam can also create quantum emitter at the edge periphery with a 31% success rate.[15] While initial research showed no pronounced dependence of type II quantum emitters on applied magnetic field (*g*-factor close to zero),[16] the recent discovery of a pronounced anisotropic photoluminescence pattern in a magnetic field for type I quantum emitters that displays a spin-dependent intersystem crossing between triplet and singlet manifolds is promising toward optically addressable spin states.[17]

To this end, integration with cavity or waveguide modes is required to enable ideally lossless transduction of quantum light states on a chip. With the goal of enhancing the brightness of the single-photon emitter (SPE) in hBN coupling to plasmonic cavities modes was recently reported, giving rise to a 2.6-fold intensity enhancement when coupled to the lattice modes of a plasmonic nanoparticle array[18] and a 4-fold intensity enhancement when coupled to dimer gap-mode cavities.[19] While the light enhancement is only modest, the plasmonic cavities also require a rotational control of the in-plane dipole of the color centers with respect to the plasmonic mode orientation, in addition to spatial and spectral matching.

Received: March 13, 2019
Accepted: May 29, 2019
Published: May 29, 2019

DOI: 10.1021/acsnano.9b01996
ACS Nano 2019, 13, 6992–6997

Figure 1. Schematic of MDA cavity design and FDTD simulation of far-field emission. (a) Schematic of the on-chip MDA device which consists of a planar silver mirror, polystyrene (PS) trenches to create embedded air gaps, a planar PS layer with embedded hBN quantum emitter, and a sapphire outcoupling layer. (b) Three temporal snapshots of the MDA mode evolution in a cross-section view with dipole emitter placed over the air-gap region. (c) Polar plot of far-field emission profile for the dipole emission from hBN on the Si/SiO_2 substrate with a PS layer attached but without the planar Ag mirror (red trace, uncoupled) and MDA mode on top of the air-gap (blue trace, coupled). Gray lines illustrate the opening angle of the objective (NA=0.55).

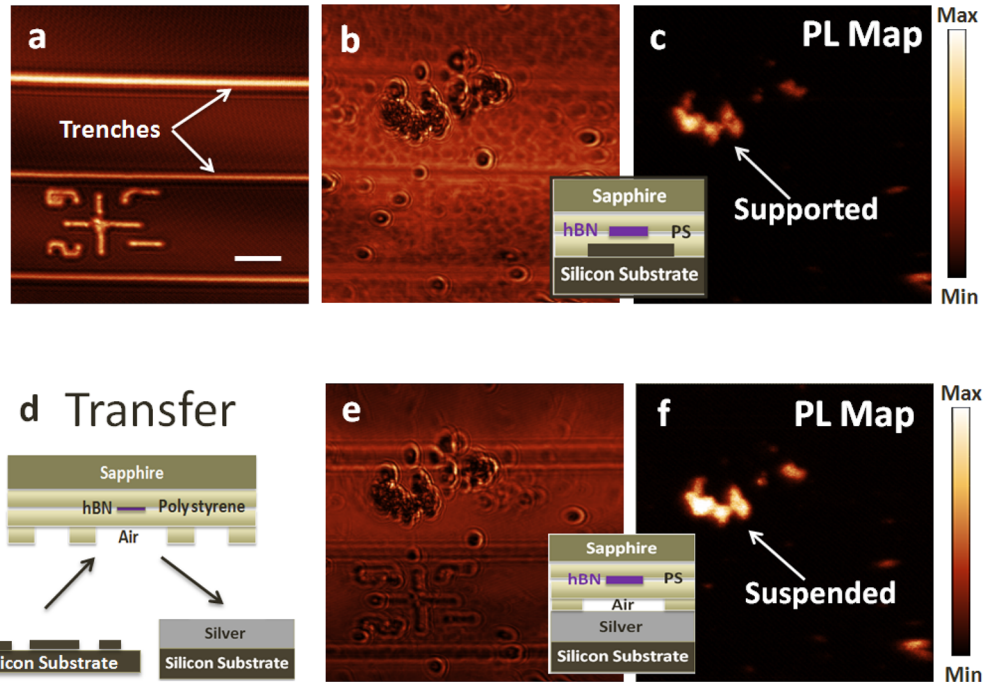

Figure 2. PL mapping of the quantum emitter emission in the uncoupled and coupled state. (a) Laser reflection scan of the silicon/SiO_2 substrate containing etched trenches (bright contrast) and a numbered cross hair marker. (b, e) Laser stray light scan through the sapphire layer illustrating that the spatial location of embedded hBN nanoflakes can be traced before and after forming the full MDA cavity mode. (c, f) Corresponding hyperspectral PL scan filtered over the zero-phonon region illustrating that the same emitters residing over the air gaps are significantly brighter. (d) Transfer scheme for the hBN nanoflakes that allows accessing both uncoupled and coupled quantum emitters. Scale bar is 10 μm.

In contrast, metallo-dielectric antennas (MDAs) are appealing alternatives to integrate hBN quantum emitters, since they feature near-unity light collection efficiency (LCE) ranging from 92 to 99%[20−26] and support arbitrary dipole orientation, as recently shown for color centers in diamond.[27,28]

Here, we demonstrate a scheme to embed hBN quantum emitters into on-chip arrays of MDAs that provide LCEs up to 98%, *i.e.*, a 7-fold enhancement compared to bare quantum emitters. Room-temperature quantum light emission in the 700 nm band is characterized with single-photon emission rates into the first lens up to 44 MHz under continuous excitation and up to 10 MHz under 80 MHz pulsed excitation (0.13 photons per trigger pulse) into a narrow output cone (±15°) that facilitates fiber butt-coupling. We furthermore provide here a direct measurement of the quantum yield under pulsed excitation with values of 6−12% for hBN nanoflakes.

RESULTS AND DISCUSSION

To achieve near unity LCE of embedded quantum emitters on-chip we designed planar MDAs by following the refractive index rule $n_1 < n_2 < n_3$ for a stack of three dielectric layers on top of a metal mirror, as originally introduced by Lee *et al.*[20] A schematic of the MDA cavity is shown in Figure 1a. To create air-gaps (n_1 = 1) against a metal mirror on-chip we first patterned a layer of polystyrene (PS, n_2 = 1.56) *via* release from a trenched substrate (see the Methods). The MDA was assembled utilizing layer transfer techniques (see Figure S1). As the first step, the patterned PS layer was transferred onto a

DOI: 10.1021/acsnano.9b01996
ACS Nano 2019, 13, 6992−6997

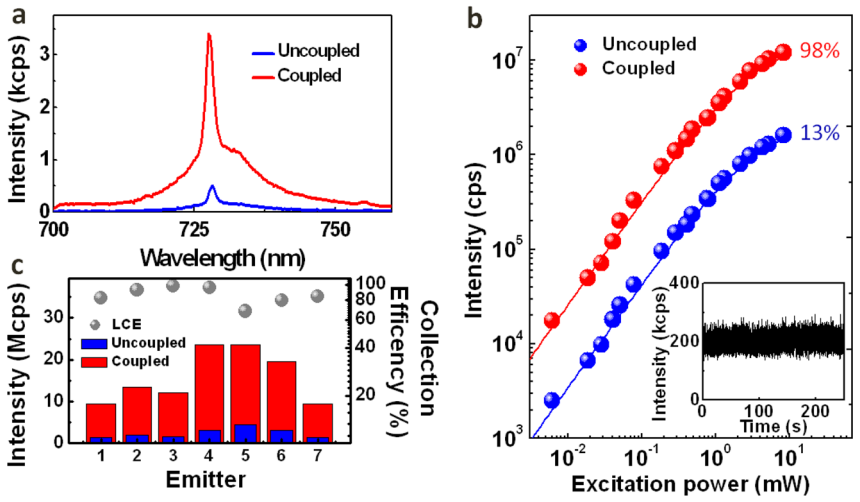

Figure 3. Demonstration of enhanced light collection efficiency *via* MDA mode coupling. (a) PL spectra of the same emitter for the uncoupled (blue trace) and coupled state (red trace) recorded under the same pump power. (b) Spectrally integrated PL intensity *versus* pump power for the uncoupled (blue data points) and coupled state (red data points). Inset: Emitter intensity over time showing excellent temporal stability without blinking. (c) Statistical comparison of the integrated intensity at highest applied optical pump power recorded before (blue) and after coupling (red) to the MDA mode (left axis). The corresponding LCE is shown for each emitter (gray data points, right axis). All measurements recorded at room temperature.

planar Si/SiO_2 substrate that was coated with 200 nm Ag to form the back mirror. The activated quantum emitters hosted in hBN nanoflakes were subsequently deposited by drop casting, followed by transfer of a planar capping layer of PS and finally and outcoupling layer of sapphire (n_3 = 1.76). In these samples, quantum emitters reside in two different locations: either on top of the air gap where they are part of an MDA cavity and benefit by enhanced LCE through cavity coupling or on top of a solid PS ridge resulting in nearly the same emission properties as compared to a bare wafer.

To quantify the expected LCE values in each case, we carried out finite-difference time-domain (FDTD) simulations. In the initial design, best results were found for a PS layer thickness of 250 nm, an air-gap thickness of 300 nm, and a sapphire capping layer of 50 nm. The directional outcoupling of light from an embedded dipole emitter into the far-field through the cavity mode is illustrated in the three temporal snapshots in Figure 1b. Quantitative values for the LCE into the first lens have been determined from the far-field radiation profile shown in Figure 1c together with the light collection cone of the first lens (gray lines). The blue trace shows the dipole emission from an emitter residing in a PS layer on a Si/SiO_2 substrate, with no planar Ag mirror attached, which defines the uncoupled case in the experiment. Here light radiates into a cone of ±65° with more than half the emission propagating in the wrong direction, giving rise to a rather low LCE of 13%. This case is comparable to a bare dipole emitter on a planar SiO_2 substrate that likewise results in LCE 13%. The red trace simulates a dipole emitter residing on top of the air-gap fully coupled into the MDA mode, resulting in a rather small output cone of ±15° and a near-unity LCE reaching 99% in theory. The simulations have been carried out for a microscope objective with moderate numerical aperture (NA = 0.55, opening angle ±33°) to match the experiments. It is clear that for the coupled case a simple lens or an optical fiber with typical NA of 0.15 is already enough to collect the entire emission from the embedded emitter, which is one of the key advantages of the MDA cavity.

In our measurement scheme, it is possible to study the same quantum emitter in hBN before and after coupling to the MDA mode in order to determine the LCE enhancement without relying on ensemble averages. To this end, we have first characterized the uncoupled case by recording hyperspectral PL images when they are supported on SiO_2. Figure 2a shows a laser reflectivity scan of a silicon wafer that contains trenches and markers that were etched into the wafer. The deposition of the first PS layer backfills the trenches and the drop-cast hBN nanoflakes reside on a planar PS layer that was capped with a second PS layer and a sapphire wafer to enable transfer. Figure 2b shows the outline of the nanoflakes and Figure 2c is the corresponding hyperspectral PL map filtered over the quantum emitter emission spectrum. The quantum emitters are clearly visible in this planar device configuration that has a rather limited LCE of 13%. As a next step we carried out a transfer process that releases the sapphire/PS stack from the Si wafer and places it on a planar metal mirror, thereby trapping air-gaps that form the MDA mode as depicted in Figure 2d. As shown in the reflected laser scan of Figure 2e, the material remains intact through the transfer process. The corresponding hyperspectral PL map for this device configuration reveals significantly brighter quantum emitter intensity when they are located over the air gap and when pumped with the same laser power (Figure 2f). This is consistent with the expectation of LCE = 99% for this case. Note that the intensity enhancement occurs within the entire suspended area (>100 μm), which significantly relaxes spatial alignment requirements between emitter and mode.[25,26]

To quantify the performance of the MDA we focus now on individual quantum emitters and track their spectral properties before and after coupling (Figure 3a). It is apparent that the MDA cavity enhances the entire spectrum uniformly without spectral distortion (see Figure S2), as expected since FDTD simulations show near unity LCE is achieved over about 100 nm bandwidth. The dipole orientation of the quantum emitter emission profile follows closely (within 20°) with the excitation profile (Figure S3). Figure 3b shows the saturation behavior of an effective two-level system that is populated

DOI: 10.1021/acsnano.9b01996
ACS Nano 2019, 13, 6992−6997

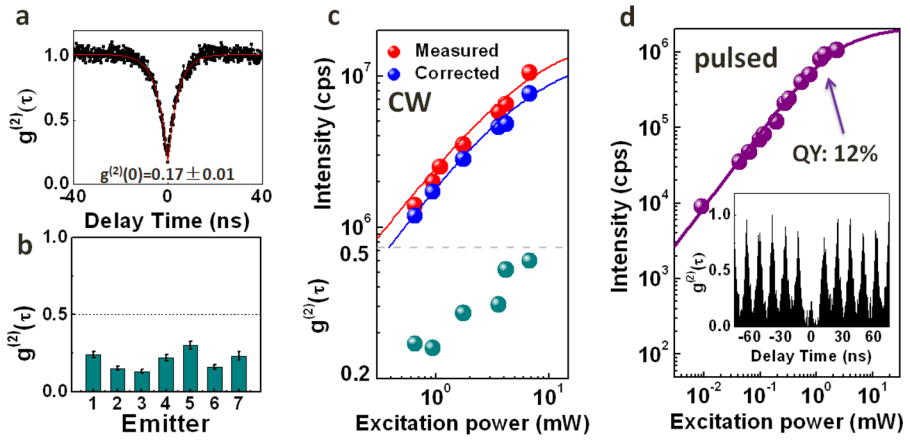

Figure 4. Characterization of single-photon source efficiency and emitter quantum yield. (a) Second-order photon correlation function $g^{(2)}(\tau)$ for the same emitter shown in Figure 3a recorded under continuous wave (CW) excitation by filtering the PL signal with a 10 nm bandpass filter. Pronounced antibunching is visible with $g^{(2)}(0) = 0.17 \pm 0.01$. (b) Exemplary antibunching values for seven embedded quantum emitters coupled to the cavity mode. The dashed line illustrates the value of $g^{(2)}(0) = 0.5$. (c) Integrated intensity *versus* pump power recorded under CW excitation (top) as well as corresponding antibunching values at zero delay time (bottom). The red data points are the total counts (signal plus background) and the blue data points are the background corrected intensities characterizing the pure single-photon emission. The solid lines are fits to the saturation equation of a two-level system. (d) Integrated intensity *versus* pump power recorded under pulsed excitation. The inset shows the $g^{(2)}(\tau)$ trace recorded near the saturation at a pump power of 340 μW, resulting in $g^{(2)}(0) = 0.22 \pm 0.04$. QY: quantum yield. All measurements recorded at room temperature.

through continuous wave pumping from an excited state. The intensity I follows a standard rate equation model with $I = I_s \cdot P/(P + P_s)$, where P is the incident pump power and $I_s = 1.6$ MHz and $P_s = 1.45$ mW are the PL intensity and pump power at saturation for the uncoupled case, respectively. For the coupled case, saturation sets in at the same pump power (*i.e.*, no Purcell effect) but with significantly increased intensity (I_s = 12.1 MHz), corresponding to an intensity enhancement factor (EF) of 7. The inset demonstrates that the PS embedded quantum emitter does not carry out any blinking at a timing resolution of 1 ms. In addition, the spectra appear stable over time with no indication of spectral diffusion (Figure S4), similar to our previous work of hBN quantum emitters that were embedded in Al_2O_3.[16]

In general, contributions to EF are expected from enhanced absorption rate, enhanced emission rate (Purcell effect), and increased LCE. As previously shown, for MDAs both enhanced absorption and Purcell effect are negligible (~10%) due to the quasi-waveguide mode being broadband with a very large mode volume.[25] Therefore, EF predominantly reflects the achieved LCE enhancement relative to the uncoupled case (LCE = 13%). The statistical analysis of several quantum emitters before and after coupling in Figure 3c reveals measured single emitter count rates ranging from 1.5 to 4.5 MHz before coupling and up to 23.5 MHz under MDA mode coupling. From these data one can estimate an average LCE of 85% (EF = 6.54) for all studied quantum emitters, as well as an LCE reaching up to 98% (EF = 7.54) in the best case.

To verify the quantum light signature of the quantum emitter shown in Figure 3a, we carried out the second order photon correlation function $g^{(2)}(\tau)$ under continuous-wave laser excitation (Figure 4a). Pronounced single-photon antibunching is characterized by a zero-delay time value of $g^{(2)}(0) = 0.17 \pm 0.01$. Photon recovery time of $\tau_0 = 4.5$ ns are determined *via* fitting the traces with the relation $g^{(2)}(\tau) = 1 - a \exp(-|\tau|/\tau_0)$, where a quantifies the background of uncorrelated photons. The statistical histograms in Figure 4b show $g^{(2)}(\tau)$ values well below 0.5 (black dash line), ranging from 0.07 ± 0.01 to 0.33 ± 0.03, for seven emitters coupled to MDA, implying well preserved single-photon purity when embedded in the cavity mode.

In order to determine the achievable brightness of the single-photon source we measured the intensity and the corresponding $g^{(2)}(0)$ values as a function of pump power, as shown in Figure 4c. It is apparent that the purity of single-photon emission drops as the pump power increases due to the increased contribution from the background. Following Grosso *et al.*,[11] one can correct for the contribution of the multiphoton background to the underlying single-photon intensity S using the equation $S = (S + B)\sqrt{1 - g^{(2)}_{exp}(0)}$, where $g^{(2)}_{exp}(0)$ is the experimentally determined antibunching value (green data points). When pumped near saturation, raw emitter count rates up to 10.5 MHz were determined (red data points), corresponding to $(S + B)$. Using the experimentally determined value of $g^{(2)}_{exp}(0) = 0.47 \pm 0.05$ at the highest pump power, one can estimate a rate of pure single-photon generation of 7.6 MHz (blue data points). Furthermore, considering that the detection efficiency of our setup is limited to 17%, one can estimate a single-photon emission rate into the first lens up to 44 MHz, which is comparable to the values reported for cavity-coupled quantum dots,[29] but was here achieved at room temperature and under near-unity light collection efficiency.

In addition, we determined the performance of the single-photon source under pulsed excitation. On the one hand, this is the required mode that creates triggered single-photons on demand as required for application in quantum cryptography. On the other hand, one can determine the underlying quantum yield (QY) of the single-photon emitter, which can be calculated from the measured number of single-photons emitted in the saturation-regime normalized to the laser repetition rate.[30,31] In the ideal case of unity QY and unity LCE, each laser pulse generates one photon and the measured count rate must match the laser repetition rate after correcting for the external detection efficiency of the system. Since LCE is

DOI: 10.1021/acsnano.9b01996
ACS Nano 2019, 13, 6992−6997

close to unity in our MDAs, reduced count rates in the experiment directly determine the emitter QY. Figure 4d shows the corresponding intensity data under pulsed excitation with a repetition rate of 80 MHz. The inset demonstrates good antibunching with $g^{(2)}_{exp}(0) = 0.22 \pm 0.04$ even in the saturation regime ($P > 300\ \mu W$). From these data, one can infer a QY of 12% for the best case, while values typically vary between 6 and 12% for other emitters. Apparently, the hBN nanoflakes utilized in this study are dominated by a nonradiative decay channel under room temperature conditions.

CONCLUSIONS

In conclusion, our demonstration of on-chip MDA cavities that embed hBN quantum emitters provides here a room-temperature quantum light source with single-photon emission rates into the first lens up to 44 MHz under continuous excitation and up to 10 MHz under 80 MHz pulsed excitation (0.13 photons per trigger pulse) and single-photon purity up to 17% into a narrow output cone of ±15° and with unity light collection efficiency (LCE = 98%). We furthermore provided direct measurement of the emitter QY in hBN nanoflakes (12%), leaving room for an *a priori* 8-fold improvement of the material quality of color centers in hBN host crystals in future work. Applications in the form of on-chip quantum random number generators are readily available and benefit by the emission in the visible range due to the low-cost single-photon detectors based on silicon technology. In contrast, their use in fiber-based quantum cryptography would still require lossy quantum frequency conversion of the visible light emission to match the standard telecom bands, in contrast to other color centers in SiC[32] and GaN[33] that readily emit in the 1300 nm bands, unless free-space quantum key distribution is targeted. Importantly, the nearly lossless interface between photons and solid-sate quantum emitters provided by the MDA integration enables efficient spin-photon interfaces, particularly in light of recent magneto-optical signatures of spin states in hBN.[17]

METHODS

Sample Preparation. Nanoflakes of hBN were dispersed in ethanol/water solution with a concentration of 5.4 mg/L (Graphene Supermarket). The lateral size of the flakes ranges between 50 and 200 nm and typically consists of 1−5 monolayers. The solution was prepared with bath sonication for 2 h at 40 ° C to create a significant density of activated color centers. To create the polymer trenches that form the MDA structures, 300 nm thick SiO_2 residing on a Si wafer was etched with an inductively coupled plasma (ICP) etcher at a rate of 10 nm/min and a plasma power of 100 W using CHF_3 gas at flow rates of 15 sccm. Etching was stopped after 30 min when the Si substrate was reached. Subsequently, polystyrene (PS) layers were spin coated (3200 rpm) for 1 min onto the SiO_2/Si substrate and baked at 65 °C for 5 min. The hBN nanoflake solution was drop casted onto the first PS layer then dried for 15 min at 65 °C and then covered with a second 250 nm thick layer of PS. A sapphire glass slide was capped onto the stack to form the high index outcoupling layer and investigated to determine the optical properties in the uncoupled state. To transfer the sapphire/PS/hBN/PS stack (uncoupled state), the substrate was floated in KOH solution for 30 min until it fully detached from the substrate. Then the polymer layers stacks were rinsed with DI water for several hours. Finally, the stacks were transferred with the trenches downward onto Si wafers that had been coated with about 200 nm silver that form the planar metal mirrors of the MDA (coupled state). For a schematic of the process flow *via* layer transfer, see Figure S1.

Optical Measurements. A 532 nm continuous wave laser focused onto the sample to a resolution-limited spot was used for optical excitation while the sample was held at room temperature. Further details of the utilized spectroscopy setup have been published in ref 16.

Photon Correlation Measurements. Photon correlation measurements were carried out under both continuous wave and pulsed excitation (80 MHz) based on a 405 nm laser diode (Picoquant). To record single-photon coincidences from the two output arms of a fiber beam splitter, a SensL timing module set at a timing jitter of 432 ps was used. To clean up the background, we used a linear polarizer in the collection path.

ASSOCIATED CONTENT

Supporting Information

The Supporting Information is available free of charge on the ACS Publications website at DOI: 10.1021/acsnano.9b01996.

Additional information on sample fabrication process flow, polarization dependence of PL intensity, normalized PL spectra, and details of system collection efficiency (PDF)

AUTHOR INFORMATION

Corresponding Author

*E-mail: strauf@stevens.edu.

ORCID

Yue Luo: 0000-0002-2757-5395

Stefan Strauf: 0000-0002-9887-7059

Notes

The authors declare no competing financial interest.

ACKNOWLEDGMENTS

S.S. acknowledges financial support by the National Science Foundation (NSF) under awards ECCS-MRI-1531237 and EFRI-ACQUIRE-1641094.

REFERENCES

(1) Toth, M.; Aharonovich, I. Single Photon Sources in Atomically Thin Materials. *Annu. Rev. Phys. Chem.* **2019**, *70*, 123−142.

(2) Tran, T. T.; Bray, K.; Ford, M. J.; Toth, M.; Aharonovich, I. Quantum Emission from Hexagonal Boron Nitride Monolayers. *Nat. Nanotechnol.* **2016**, *11*, 37−41.

(3) Kianinia, M.; Regan, B.; Tawfik, S. A.; Tran, T. T.; Ford, M. J.; Aharonovich, I.; Toth, M. Robust Solid-State Quantum System Operating at 800 K. *ACS Photonics* **2017**, *4*, 768−773.

(4) Martínez, L. J.; Pelini, T.; Waselowski, V.; Maze, J. R.; Gil, B.; Cassabois, G.; Jacques, V. Efficient Single Photon Emission from a High-Purity Hexagonal Boron Nitride Crystal. *Phys. Rev. B: Condens. Matter Mater. Phys.* **2016**, *94*, No. 121405(R).

(5) Tran, T. T.; Zachreson, C.; Berhane, A. M.; Bray, K.; Sandstrom, R. G.; Li, L. H.; Taniguchi, T.; Watanabe, K.; Aharonovich, I.; Toth, M. Quantum Emission from Defects in Single-Crystalline Hexagonal Boron Nitride. *Phys. Rev. Appl.* **2016**, *5*, 034005.

(6) Jungwirth, N. R.; Calderon, B.; Ji, Y.; Spencer, M. G.; Flatté, M. E.; Fuchs, G. D. Temperature Dependence of Wavelength Selectable Zero-Phonon Emission from Single Defects in Hexagonal Boron Nitride. *Nano Lett.* **2016**, *16*, 6052−6057.

(7) Chejanovsky, N.; Rezai, M.; Paolucci, F.; Kim, Y.; Rendler, T.; Rouabeh, W.; Fávaro de Oliveira, F.; Herlinger, P.; Denisenko, A.; Yang, S.; Gerhardt, I.; Finkler, A.; Smet, J. H.; Wrachtrup, J. Structural Attributes and Photodynamics of Visible Spectrum Quantum Emitters in Hexagonal Boron Nitride. *Nano Lett.* **2016**, *16*, 7037−7045.

(8) Ngoc My Duong, H.; Nguyen, M. A. P.; Kianinia, M.; Ohshima, T.; Abe, H.; Watanabe, K.; Taniguchi, T.; Edgar, J. H.; Aharonovich, I.; Toth, M. Effects of High Energy Electron Irradiation on Quantum Emitters in Hexagonal Boron Nitride. *ACS Appl. Mater. Interfaces* **2018**, *10*, 24886−24891.

DOI: 10.1021/acsnano.9b01996
ACS Nano 2019, 13, 6992−6997

(9) Xu, Z. Q.; Elbadawi, C.; Tran, T. T.; Kianinia, M.; Li, X.; Liu, D.; Hoffman, T. B.; Nguyen, M.; Kim, S.; Edgar, J. H.; Wu, X. Single Photon Emission from Plasma Treated 2D Hexagonal Boron Nitride. *Nanoscale* **2018**, *10*, 7957−7965.
(10) Tran, T. T.; Elbadawi, C.; Totonjian, D.; Lobo, C. J.; Grosso, G.; Moon, H.; Englund, D. R.; Ford, M. J.; Aharonovich, I.; Toth, M. Robust Multicolor Single Photon Emission from Point Defects in Hexagonal Boron Nitride. *ACS Nano* **2016**, *10*, 7331−7338.
(11) Grosso, G.; Moon, H.; Lienhard, B.; Ali, S.; Efetov, D. K.; Furchi, M. M.; Jarillo-Herrero, P.; Ford, M. J.; Aharonovich, I.; Englund, D. Tunable and High Purity Room-Temperature Single Photon Emission from Atomic Defects in Hexagonal Boron Nitride. *Nat. Commun.* **2017**, *8*, 705.
(12) Noh, G.; Choi, D.; Kim, J.-H.; Im, D.-G.; Kim, Y.-H.; Seo, H.; Lee, J. Stark Tuning of Single-Photon Emitters in Hexagonal Boron Nitride. *Nano Lett.* **2018**, *18*, 4710−4715.
(13) Mendelson, N.; Xu, Z. Q.; Tran, T. T.; *etc.* Bottom up Engineering of Near-identical Quantum Emitters in Atomically Thin Materials. *arXiv*:1806.011, 2018. https://arxiv.org/abs/1806.01199 (accessed Jun 4, 2018).
(14) Proscia, N. V.; Shotan, Z.; Jayakumar, H.; Reddy, P.; Dollar, M.; Alkauskas, A.; Doherty, M.; Meriles, C. A.; Menon, V. M. Near-Deterministic Activation of Room Temperature Quantum Emitters in Hexagonal Boron Nitride. *Optica* **2018**, *5*, 1128−1134.
(15) Ziegler, J.; Klaiss, R.; Blaikie, A.; Miller, D.; Horowitz, V. R.; Alemán, B. J. Deterministic Quantum Emitter Formation in Hexagonal Boron Nitride *via* Controlled Edge Creation. *Nano Lett.* **2019**, *19*, 2121−2127.
(16) Li, X.; Shepard, G. D.; Cupo, A.; Camporeale, N.; Shayan, K.; Luo, Y.; Meunier, V.; Strauf, S. Nonmagnetic Quantum Emitters in Boron Nitride with Ultranarrow and Sideband-Free Emission Spectra. *ACS Nano* **2017**, *11*, 6652−6660.
(17) Exarhos, A. L.; Hopper, D. A.; Patel, R. N.; Doherty, M. W.; Bassett, L. C. Magnetic-Field-Dependent Quantum Emission in Hexagonal Boron Nitride at Room Temperature. *Nat. Commun.* **2019**, *10*, 222.
(18) Tran, T. T.; Wang, D.; Xu, Z.-Q.; Yang, A.; Toth, M.; Odom, T. W.; Aharonovich, I. Deterministic Coupling of Quantum Emitters in 2D Materials to Plasmonic Nanocavity Arrays. *Nano Lett.* **2017**, *17*, 2634−2639.
(19) Nguyen, M.; Kim, S.; Tran, T. T.; Xu, Z.-Q.; Kianinia, M.; Toth, M.; Aharonovich, I. Nanoassembly of Quantum Emitters in Hexagonal Boron Nitride and Gold Nanospheres. *Nanoscale* **2018**, *10*, 2267−2274.
(20) Lee, K. G.; Chen, X. W.; Eghlidi, H.; Kukura, P.; Lettow, R.; Renn, A.; Sandoghdar, V.; Götzinger, S. A Planar Dielectric Antenna for Directional Single-Photon Emission and Near-Unity Collection Efficiency. *Nat. Photonics* **2011**, *5*, 166−169.
(21) Chen, X.-W.; Agio, M.; Sandoghdar, V. Metallodielectric Hybrid Antennas for Ultrastrong Enhancement of Spontaneous Emission. *Phys. Rev. Lett.* **2012**, *108*, 233001.
(22) Chu, X.-L.; Brenner, T. J. K.; Chen, X.-W.; Ghosh, Y.; Hollingsworth, J. A.; Sandoghdar, V.; Götzinger, S. Experimental Realization of an Optical Antenna Designed for Collecting 99% of Photons from a Quantum Emitter. *Optica* **2014**, *1*, 203−208.
(23) Chu, X.-L.; Götzinger, S.; Sandoghdar, V. A Single Molecule as a High-Fidelity Photon Gun for Producing Intensity-Squeezed Light. *Nat. Photonics* **2017**, *11*, 58−62.
(24) Morozov, S.; Gaio, M.; Maier, S. A.; Sapienza, R. Metal−Dielectric Parabolic Antenna for Directing Single Photons. *Nano Lett.* **2018**, *18*, 3060−3065.
(25) Shayan, K.; Rabut, C.; Kong, X.; Li, X.; Luo, Y.; Mistry, K. S.; Blackburn, J. L.; Lee, S. S.; Strauf, S. Broadband Light Collection Efficiency Enhancement of Carbon Nanotube Excitons Coupled to Metallo-Dielectric Antenna Arrays. *ACS Photonics* **2018**, *5*, 289−294.
(26) Shayan, K.; He, X.; Luo, Y.; Rabut, C.; Li, X.; Hartmann, N. F.; Blackburn, J. L.; Doorn, S. K.; Htoon, H.; Strauf, S. Suppression of Exciton Dephasing in Sidewall-Functionalized Carbon Nanotubes Embedded into Metallo-Dielectric Antennas. *Nanoscale* **2018**, *10*, 12631−12638.
(27) Karamlou, A.; Trusheim, M. E.; Englund, D. Metal-Dielectric Antennas for Efficient Photon Collection from Diamond Color Centers. *Opt. Express* **2018**, *26*, 3341−3352.
(28) Zheng, J.; Liapis, A. C.; Chen, E. H.; Black, C. T.; Englund, D. Chirped Circular Dielectric Gratings for Near-Unity Collection Efficiency from Quantum Emitters in Bulk Diamond. *Opt. Express* **2017**, *25*, 32420−32435.
(29) Strauf, S.; Stoltz, N. G.; Rakher, M. T.; Coldren, L. A.; Petroff, P. M.; Bouwmeester, D. High-Frequency Single-Photon Source with Polarization Control. *Nat. Photonics* **2007**, *1*, 704−708.
(30) Luo, Y.; Shepard, G. D.; Ardelean, J. V.; Rhodes, D. A.; Kim, B.; Barmak, K.; Hone, J. C.; Strauf, S. Deterministic Coupling of Site-Controlled Quantum Emitters in Monolayer WSe_2 to Plasmonic Nanocavities. *Nat. Nanotechnol.* **2018**, *13*, 1137−1142.
(31) Luo, Y.; Ahmadi, E. D.; Shayan, K.; Ma, Y.; Mistry, K.; Zhang, C.; Hone, J.; Blackburn, J. L.; Strauf, S. Purcell-Enhanced Quantum Yield from Carbon Nanotube Excitons Coupled to Plasmonic Nanocavities. *Nat. Commun.* **2017**, *8*, 1413.
(32) Wang, J.; Zhou, Y.; Wang, Z.; Rasmita, A.; Yang, J.; Li, X.; von Bardeleben, H. J.; Gao, W. B. Bright Room Temperature Single Photon Source at Telecom Range in Cubic Silicon Carbide. *Nat. Commun.* **2018**, *9*, 4106.
(33) Zhou, Y.; Wang, Z.; Rasmita, A.; Kim, S.; Berhane, A.; Bodrog, Z.; Adamo, G.; Gali, A.; Aharonovich, I.; Gao, W. B. Room Temperature Solid-State Quantum Emitters in the Telecom Range. *Sci. Adv.* **2018**, *4*, No. eaar3580.

DOI: 10.1021/acsnano.9b01996
ACS Nano 2019, 13, 6992−6997